Dyes and Pigments 162 (2019) 43–51

Contents lists available at ScienceDirect

Dyes and Pigments

journal homepage: www.elsevier.com/locate/dyepig

The regulation of π-bridge of indacenodithiophene-based donor-π-acceptor conjugated polymers toward efficient polymer solar cells

Xudong Gao[a,b], Yonghai Li[b], Lu Yu[a], Feng Hou[a], Tingting Zhu[a], Xichang Bao[b], Feng Li[c], Mingliang Sun[a,*], Renqiang Yang[b]

[a] School of Material Science and Engineering, Ocean University of China, Qingdao, 266100, China
[b] CAS Key Laboratory of Bio-based Materials, Qingdao Institute of Bioenergy and Bioprocess Technology, Chinese Academy of Sciences, Qingdao, 266101, China
[c] Key Laboratory of Rubber-Plastics of Ministry of Education/Shandong Province, School of Polymer Science and Engineering, Qingdao University of Science & Technology, Qingdao, 266042, China

ARTICLE INFO

Keywords:
Conjugated polymers
Polymer solar cell
Indacenodithiophene (IDT)
π-bridge
Power conversion efficiency

ABSTRACT

The instinct feature of π-bridges of donor-π-acceptor (D-π-A) conjugated polymers plays a critical role in tailoring the polymer basic properties as well as the photovoltaic performance. In this work, we designed two new D-π-A polymers PSeBDDIDT and PTzBDDIDT based on donor unit indacenodithiophene (IDT), acceptor unit benzo[1,2-c:4,5-c']dithiophene-4,8-dione (BDD) with varying π-conjugated bridges of selenophene and thiazole units. Compared to the counterpart polymer PThBDDIDT with thiophene π-bridge, polymers PSeBDDIDT and PTzBDDIDT exhibited enhanced intermolecular interactions, expanded absorption range and better molecular planarity arising from the suppressed steric hindrance between the respective bridge and the adjacent BDD moiety. Conventional polymer solar cells were fabricated with $PC_{71}BM$ as the acceptor. The results witness a greatly improved efficiency for PSeBDDIDT based solar cell compared to PThBDDIDT based counterpart device (7.04%). As a result, the champion PCE of 8.65% was recorded with V_{OC} of 0.899 V, J_{SC} of 16.04 mA cm^{-2} and FF of 0.60. It is worth highlighting that this is the highest efficiency among all IDT-based polymeric donors reported till now. As a contrast, the devices fabricated from PTzBDDIDT demonstrated a low efficiency of 2.75%, with increased V_{OC} of 0.968 V, J_{SC} of 8.12 mA cm^{-2} and FF of 0.35. The inferior photocurrent and fill factor of PTzBDDIDT based device was in accord with the poor exciton dissociation probability (38%) and low hole and electron charge transport inside the polymer solar cell. In conclusion, this work demonstrates a state of the art IDT-based polymeric donor with selenophene π-bridge and the importance of rational regulation of π-bridges on polymer properties and photovoltaic efficiency of polymer solar cells.

1. Introduction

Organic semiconductors, including conjugated small molecules and polymers, have been intensively investigated for their promising applications in various flexible optoelectronic devices [1,2]. Among them, bulk-heterojunction (BHJ) polymer solar cells (PSCs) are considered fairly important for the generation of green energy [3–6]. As for the active layer of PSCs, the devices made by combination of polymeric donor materials and small molecular acceptor materials (fullerene-based [6,6]-phenyl-(C_{61} or C_{71})butyric acid methyl ester and fuse-ring non-fullerene acceptors) are proved to be the most efficient polymer solar cells. The power conversion efficiencies (PCEs) non-fullerene BHJ PSCs have reached 14% up to now, signifying the great promise of practical application [7]. Thus the exploration of superior polymeric donor materials will greatly advance the PSCs development. Donor-π-acceptor (D-π-A) conjugated polymers composed of electron-donating unit (D), electron-accepting unit (A) as well as the π-bridges are widely utilized as polymeric donors due to their tunable frontier energy levels, absorption spectra and charge mobilities [8–12]. Generally, the basic opto-electronic properties of D-π-A polymers are mainly influenced by the D and A moieties. Nevertheless, the π-bridge species also play a considerable role in releasing the steric strain of polymer backbone, modifying the molecular conformation and other behaviors.

In the design of D-π-A polymeric donors, thiophene is the most commonly and successfully used π-bridge for smaller distortion with adjacent groups, moderate electronegativity and intermolecular S···S non-covalent weak interactions. Benzene unit is seldom utilized as the π-bridge for the great steric hindrance between the H atom in benzene

* Corresponding author.
E-mail addresses: liyh@qibebt.ac.cn (Y. Li), mlsun@ouc.edu.cn (M. Sun), yangrq@qibebt.ac.cn (R. Yang).

https://doi.org/10.1016/j.dyepig.2018.10.008
Received 29 August 2018; Received in revised form 6 October 2018; Accepted 6 October 2018
Available online 09 October 2018
0143-7208/

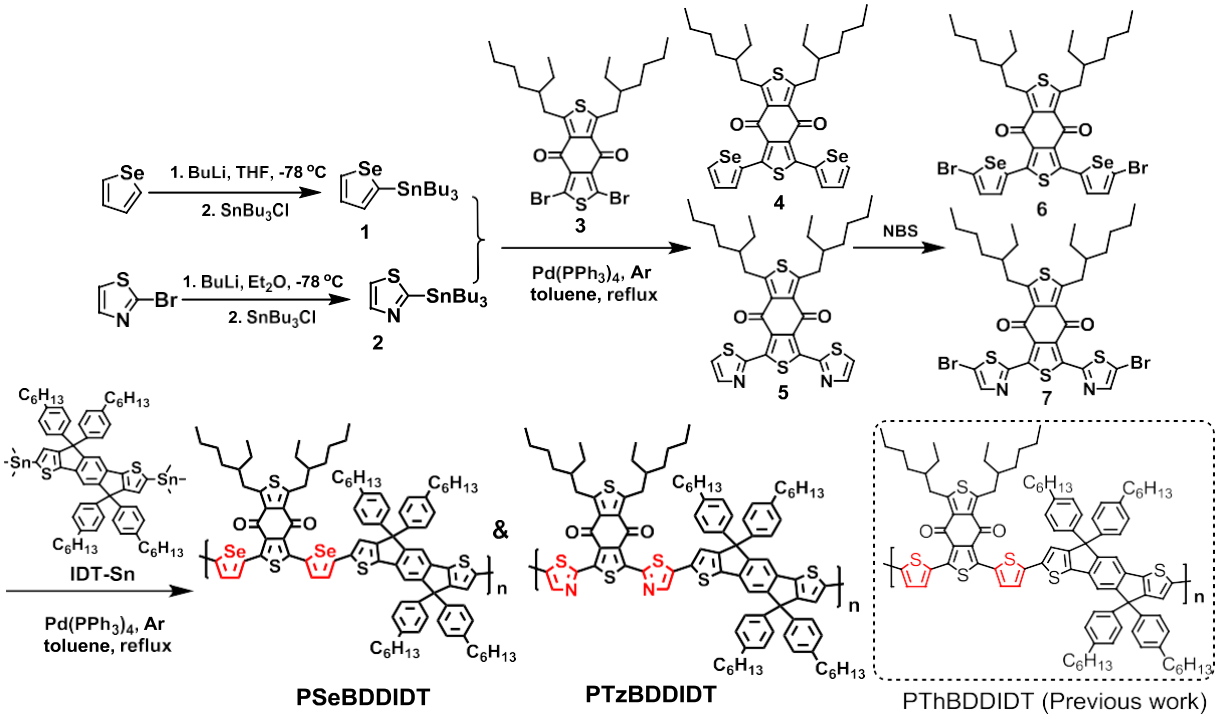

Scheme 1. The chemical structures and synthetic approaches of polymers PSeBDDIDT and PTzBDDIDT.

and the adjacent groups, generally hurting the π-π stacking and intermolecular interactions and producing a hypochromic shifted absorption [13–15]. The exception was, in some cases the over-strong intermolecular interactions of polymeric donors could lead to strong phase-separation behavior in donor/acceptor blends, thus the weakened intermolecular interaction and hypochromic shifted absorption of polymers especially combined with the narrow band-gap acceptors could produce improved photovoltaic performance [16]. Belonging to the chalcogen family, selenophene unit usually possesses similar chemical and physical properties to the widely used thiophene unit. However, selenophene unit also has some intrinsic properties making it a promising π-bridge in D-π-A type polymers and small molecules. Specifically, selenophene has lower aromaticity than thiophene which can increase the quinoidal resonance form in the ground state of the resulting polymers [17–20]. For example, it has been documented that polyselenophene is prone to have quinoidal population higher than that of polythiophene, producing more planar backbone and longer effective conjugation length [21]. This makes selenophene unit a unique π-bridge in design of D-π-A type polymers with narrower band-gaps and enhanced light-harvesting ability. For instance, Li et al. found that when changing the π-conjugated bridge from thiophene to selenophene units in PBDT-BDD system, the polymer PBPD-Se exhibits superior efficiency than the thiophene counterpart PBPD-Th with greatly improved short-circuit current density (J_{SC}) from 12.4 to 14.9 mA cm^{-2}, and the overall PCE increased to 9.8% after additive treatment [22]. Compared to electron-rich thiophene and selenophene, there is a significant difference for hetero-cyclic thiazole unit as the π-bridge because of its electron-deficient nature. The electronegative nitrogen atom in thiazole can reduce the frontier energy levels of its resulting donor materials, which will be beneficial for achieving a high open-circuit voltage (V_{OC}) of solar cells [23–26]. Previously, we reported two isomeric thienothiophene-based copolymers and investigate the different orientations of the thiazole group as the π-bridge. The results show that the orientations of π-bridge also play a critical role on the photovoltaic performance and eventually a superior PCE of 9.72% was measured [27]. Recently, Huang et al. developed a novel type of IDT-based small molecular acceptor IDT-Tz, using thiazole as the π-bridge. By employing thiazole unit as the π-bridge, nitrogen/sulfur noncovalent conformational locks were introduced to enhance the rigidity and planarity of the backbone. According to their report, the solar cells based on the IDT-Tz electron acceptor exhibit greatly improved PCE of 8.4% higher than the thiophene counterpart IDT-T (4.1%) [28].

With regard to the progress of organic solar cells, it should be mentioned that the fuse-ring A-D-A fullerene-free acceptors (IDIC and ITIC for instance) with indacenodithiophene (IDT) and indacenodithieno[3,2-*b*]thiophene (IDTT) as the core backbones have generated highly efficient PSCs. However, as the electron-rich building blocks, the efficiencies of IDT and IDTT based D-π-A type polymers are inferior to the respective acceptors [29–36]. Zheng's group reported a wide band-gap polymer PIDTBTO-TT with PCE up to 8.15%, which ever represented the highest solar cell efficiency achieved with IDT-based polymers [32]. In our previous work, we designed a couple of D-π-A type polymers with IDT or IDTT as the D moiety, weak electron-withdrawing moiety benzo[1,2-c:4,5-c']dithiophene-4,8-dione (BDD) as the A moiety and thiophene as π-bridge.[37] We found the polymer PBDDIDT exhibits higher PCE than that of PBDDIDTT. Besides, the current densities of the solar cells were around 10 mA cm^{-2}, and the fill factor (FF) of the devices raised along with the increase of $PC_{71}BM$ content. Finally, the optimal efficiency of 7.04% was measured with 80% content of $PC_{71}BM$ in active layer [37]. On the basis of the design of D-π-A polymers discussed above, an alternative strategy to optimize the photo-voltage, photo-current and even PCEs of IDT-based polymer solar cells is to tailor the properties of π-bridges for the optimization of the polymer absorption, energy levels as well as the molecular conformations.

Hence, in this work, we further employed the selenophene and thiazole units as π-conjugated bridges and synthesized two new D-π-A polymers, named PSeBDDIDT and PTzBDDIDT, respectively, with IDT unit as the donor part and BDD unit as the acceptor part. In order to investigate the regulation of different π-bridges on the material properties and photovoltaic performance, some results of the analogue polymer PThBDDIDT (to make a more direct comparison, PBDDIDT in previous report with thiophene as the π-bridge was labeled as PThBDDIDT in this work) were extracted directly from the previous

report and some unexplored properties of PThBDDIDT are further investigated here. The chemical structures of three polymers are shown in Scheme 1. The results show both polymers PSeBDDIDT and PTzBDDIDT reveal better backbone planarity and enhanced molecular interactions than PThBDDIDT. Meanwhile, the absorption spectra of PSeBDDIDT are largely red-shifted with respect to the counterpart polymer PThBDDIDT, contributing to the raised J_{SC} of PSCs. Eventually, PCE up to 8.65% was recorded with V_{OC} of 0.899 V, J_{SC} of 16.04 mA cm^{-2} and FF of 0.60. To the best of our knowledge, the PCE of PSeBDDIDT based PSC exhibits the highest efficiency among all the IDT-based polymeric donors. However, there are quite different results obtained for polymer PTzBDDIDT. The decreased HOMO level of PTzBDDIDT compared to PThBDDIDT declares upshifted V_{OC} value. Nonetheless, the photovoltaic devices of polymer PTzBDDIDT demonstrate inferior properties with the champion PCE of 2.75%, V_{OC} of 0.968 V, J_{SC} of 8.12 mA cm^{-2} and FF of 0.35. The BHJ morphologies of PTzBDDIDT/$PC_{71}BM$ show uniform film and nanoscale phase-separation which should not be responsible for the low current density and fill factor. The results of exciton dissociation studies show that PTzBDDIDT based device suffers from insufficient exciton dissociation with exciton dissociation probability [P_{diss}(E,T)] of 38%, which may be blamed to the narrow LUMO difference between the donor and acceptor. Thus, the rational modification of π-bridge is crucial for the D-π-A polymer fabricated polymer solar cells.

2. Materials and methods

2.1. Synthesis ofmaterials

All solvents such as THF and toluene were purchased from Alfa-Aesar and Sigma-Aldrich, some starting chemicals were purchased from J&K and TCI. The synthetic routes for the new polymers are shown in Scheme 1 and the synthesis details are described below.

Synthesis of tributyl(selenophen-2-yl)stannane (1): Selenophene (1.00 g, 7.63 mmol) was dissolved in dry THF (30 mL) and placed under a argon atmosphere. The solution was placed into an ice bath and stirred while 1.6 M n-butyllithium in hexane (4.75 mL, 7.63 mmol) was added dropwise. The mixture was stirred for another 2.0 h at −78 °C, then tributylchlorostannane (2.20 mL, 7.63 mmol) was added. The solution was warmed to room temperature and stirred overnight. Then it was poured into water and extracted with ether (3 × 50 mL). The organic phase was combined and dried over anhydrous Na_2SO_4. After removal of the solvent, the crude product (1) was utilized for the next step without further purification.

Synthesis of 2-(tributylstannyl)thiazole (2): 2-bromothiazole (1.64 g, 10 mmol) was dissolved in dry ether (30 mL) and placed under a argon atmosphere. The solution was cooled to −78 °C and stirred while 1.6 M n-butyllithium in hexane (6.60 mL, 10.50 mmol) was added dropwise. The mixture was stirred for another 2.0 h at −78 °C, then tributylchlorostannane (2.90 mL, 10 mmol) was added. The solution was warmed to room temperature and stirred overnight. Then it was poured into water and extracted with ether (3 × 50 mL). The organic phase was combined and dried over anhydrous Na_2SO_4. After removal of the solvent, the crude product (2) was utilized for the next step without further purification.

Synthesis of compounds 4 and 5: A solution of 2BrBDD (3) (1 g, 1.66 mmol), tributyl(selenophen-2-yl)stannane or 2-(tributylstannyl) thiazole (10 mmol, 6eq) and a catalytic amount of Pd $(PPh_3)_4$ (0.05 eq) in dry toluene (40 mL) was heated at reflux for 24 h under argon atmosphere. After the reaction, the solvent was evaporated under vacuum and the residue was subjected to column chromatography on silica gel with petroleum ether/CH_2Cl_2 (v/v, 1/1) for compound 4, pure CH_2Cl_2 for compound 5 as the eluent. Compound 4 was obtained as orange solids (1.04 g, yield: 89.6%). Compound 5 was obtained as yellow solids (0.98 g, yield: 96.5%). For compound 4: ^{1}H NMR (600 MHz, $CDCl_3$, δ ppm) 8.29 (d, J = 5.8 Hz, 2H), 7.97 (d, J = 3.9 Hz, 2H), 7.39 (dd, J = 5.7, 4.1 Hz, 2H), 3.36–3.26 (m, 4H), 1.84–1.73 (m, 2H), 1.45–1.23 (m, 15H), 0.92 (dt, J = 32.3, 7.1 Hz, 12H). ^{13}C NMR (151 MHz, $CDCl_3$, δ ppm) 178.23, 153.45, 145.19, 137.42, 137.29, 133.07, 132.85, 131.32, 129.68, 41.33, 33.80, 32.96, 29.87, 26.20, 23.19, 14.29, 11.04. MS (MALDI-TOF): m/z 705.1 $(M+1)^+$. For compound 5: ^{1}H NMR (600 MHz, $CDCl_3$, δ ppm): 7.98 (d, J = 3.2 Hz, 2H), 7.57 (d, J = 3.2 Hz, 2H), 3.52–3.27 (m, 4H), 1.85–1.69 (m, 2H), 1.44–1.26 (m, 15H), 0.93 (dt, J = 24.7, 7.3 Hz, 12H). ^{13}C NMR (151 MHz, $CDCl_3$, δ ppm) 177.94, 157.70, 154.50, 145.94, 143.40, 133.03, 132.47, 123.72, 41.28, 33.76, 32.86, 28.84, 26.10, 23.06, 14.20, 10.92. MS (MALDI-TOF): m/z 611.1 $(M+1)^+$.

Synthesis of compounds 6: 4 (800 mg, 1.14 mmol) and NBS (446 mg, 2.51 mmol) were dissolved in 25 mL $CHCl_3$. After several drops of AcOH was added, the solution was stirred at room temperature under dark and monitored through TLC. When reaction was completed, the solution was washed with water for three times. Organic phase was collected, dried, concentrated and subjected to silica gel chromatograph with petroleum ether/CH_2Cl_2 (v/v, 2/1) as the eluent. After removing PE by rotary evaporator, compound 6 was obtained as red solids (784 mg, 80%). ^{1}H NMR (600 MHz, $CDCl_3$, δ ppm) 7.65 (dd, J = 4.4, 1.2 Hz, 2H), 7.34 (dd, J = 4.4, 1.1 Hz, 2H), 3.37–3.21 (m, 4H), 1.82–1.71 (m, 2H), 1.36 (m, 15H), 0.93 (dt, J = 14.0, 7.0 Hz, 12H). ^{13}C NMR (151 MHz, $CDCl_3$, δ ppm) 178.07, 154.23, 144.67, 138.24, 133.06, 132.55, 131.92, 130.71, 125.64, 41.31, 41.29, 33.87, 33.03, 29.07, 26.21, 23.22, 14.38, 11.01. MS (MALDI-TOF): m/z 862.9 $(M+1)^+$.

Synthesis of compounds 7: 5 (1.00 g, 1.64 mmol) and NBS (1.16 g, 6.55 mmol) were dissolved in 60 mL DMF. The solution was heat at 80 °C and stirred under dark and monitored through TLC. When reaction was completed, the solution was washed with water for three times. Organic phase was collected, dried, concentrated and subjected to silica gel chromatograph with CH_2Cl_2 as the eluent. After removing PE by rotary evaporator, compound 7 was obtained as bright yellow solids (694 mg, 55%). ^{1}H NMR (600 MHz, $CDCl_3$, δ ppm) 7.83 (s, 2H), 3.30 (qd, J = 14.8, 7.1 Hz, 4H), 1.87–1.70 (m, 2H), 1.42–1.25 (m, 15H), 0.94 (dt, J = 9.8, 7.2 Hz, 12H). ^{13}C NMR (151 MHz, $CDCl_3$, δ ppm) 177.68, 158.42, 155.29, 145.75, 144.57, 132.95, 132.13, 115.00, 41.32, 33.90, 33.03, 29.06, 26.23, 23.18, 14.38, 11.00. MS (MALDI- TOF): m/z 769.1 $(M+1)^+$.

Synthesis of polymers PSeBDDIDT and PTzBDDIDT: For the synthesis of polymer PSeBDDIDT, to a 25 mL flask, 2,8-bis(trimethyltin)indacenodithiophene (IDT-Sn) (123.3 mg, 0.1 mmol) and monomer 6 (86.0 mg, 0.1 mmol) were added to dry toluene (8.0 mL) and purged with argon for 30 min. Then $Pd(PPh_3)_4$ (7.0 mg, 0.0055 mmol) were added and the solution was refluxed for 24 h under argon. After cooling to room temperature, the solution was poured into methanol (100 mL) and filtered followed by subjecting to Soxhlet extraction successively with methanol, acetone and hexane as the solvents. The polymer was collected using $CHCl_3$ as the eluent and precipitated against methanol. The residue was filtered and dried under vacuum for 24 h at 40 °C to afford polymer PSeBDDIDT as blue solids with a high yield of 90%. GPC: M_n = 25.3 kDa, PDI = 2.06. T_d = 409 °C (95%, nitrogen).^{1}H NMR (600 MHz, $CDCl_3$, δ ppm): 8.10 (s), 7.85 (br), 7.41–7.09(m), 3.41–3.35 (m), 2.58 (br), 1.78 (br), 1.61–1.26 (m), 0.95–0.86 (m). Elemental analysis (%): Calc. for PSeBDDIDT: C, 73.20; H, 7.02; O, 1.99; S, 7.97; Se, 9.82. Found: C, 74.15; H, 6.32; S, 7.44. The synthetic approach of polymer PTzBDDIDT was according to the same procedure as PSeBDDIDT, except using the monomer 7. PTzBDDIDT was obtained as purple solids with a high yield of 92%. GPC: M_n = 28.5 kDa, PDI = 1.98. T_d = 404 °C (95%, nitrogen).^{1}H NMR (600 MHz, $CDCl_3$, δ ppm): 8.10 (s), 8.01–8.00 (br), 7.45–7.07 (m), 3.41–3.38 (m), 2.57 (br), 2.02 (m), 1.80 (br), 1.60–1.26 (m), 0.97–0.86 (m). Elemental analysis (%): Calc. for PTzBDDIDT: C, 76.04; H, 7.31; N, 1.85; O, 2.11; S, 12.69. Found: C, 79.45; H, 6.91; N, 1.51; S, 12.01.

2.2. Materials characterization methods

^{1}H NMR and ^{13}C NMR spectra of intermediates were collected on a Bruker AVANCE-III 600 Spectrometer at 298 K as solutions in $CDCl_3$. MALDI-TOF MS spectra were recorded with a BEFLEX III spectrometer. Elemental analysis was performed on a Carlo Erba model 1160 elemental analyzer. Gel permeation chromatography (GPC) was performed with THF as eluent and polystyrene was used as the standard. TGA measurement was performed using a SDT Q600 V20.9 Build 20 at a heating rate of 10 °C min^{-1} under a nitrogen atmosphere. UV–vis absorption spectra were measured from a Hitachi U-4100 spectrophotometer with dilute solutions and solid state films of the polymers. Cyclic voltammetry (CV) measurements were performed on a CHI660D electrochemical workstation, equipped with a three-electrode cell consisting of a platinum working electrode, a saturated calomel electrode (SCE) as reference electrode and a platinum wire counter electrode. CV measurements were carried out in anhydrous acetonitrile containing 0.1 M *n*-Bu_4NPF_6 as a supporting electrolyte under an argon atmosphere at a scan rate of 100 mV s^{-1} assuming that the absolute energy level of Fc/Fc^+ was −4.80 eV. Thin films were deposited from *o*-DCB solution onto the working electrodes. Density functional theory (DFT) calculations were confirmed by the Gaussian 09 program at the B3LYP/6-31G(d,p) level. Atomic force microscopy (AFM) images were obtained using Agilent 5400 scanning probe microscope in tapping-mode with MikroMasch NSC-15 AFM tips. XRD measurements were carried out in reflection mode at room temperature. Transmission electron microscopy (TEM) images were obtained by using a HITACHI H-7650 electron microscope with an acceleration voltage of 100 kV.

2.3. Device fabrication and evaluations

Photovoltaic devices were fabricated with a conventional device structure of ITO/PEDOT:PSS/polymer: $PC_{71}BM$/PFN/Al. The patterned ITO glass (sheet resistance = 15 Ω/square) was pre-cleaned in an ultrasonic bath of acetone and isopropyl alcohol and treated in an ultraviolet-ozone chamber (PREEN II-862) for 6 min. Then a thin layer (about 30 nm) of PEDOT:PSS was spin-coated onto the ITO glass at 4000 rpm and baked at 150 °C for 15 min. Solutions of polymer/$PC_{71}BM$ in *o*-DCB (25 mg/mL, total concentration) were stirred overnight and warmed to 50 °C for 30 min before spin-coating on the PEDOT:PSS layer to form the active layer about 100–120 nm. The thickness of the active layer was measured using a Veeco Dektak 150 profilometer. Then PFN solution (in CH_3OH) was spin-coating as electron transfer layer. Finally, Al (100 nm) metal electrode was thermal evaporated under about 4×10^{-4} Pa and the device area was 0.1 cm^2 defined by shadow mask.

The current density–voltage (*J*–*V*) characteristics were recorded with a Keithley 2400 source measurement unit under simulated 100 mW cm^{-2} irradiation from a Newport solar simulator. The external quantum efficiencies (EQEs) were analysed using a certified Newport incident photon conversion efficiency (IPCE) measurement system. The hole mobility and electron mobility were measured by space-charge-limited current (SCLC) method with a device configuration of ITO/PEDOT:PSS/active layer/MoO_3/Al and ITO/ZnO/active layer/PFN/Al structure, respectively. The SCLC is described by the Mott–Gurney law:

$$J = 9\varepsilon\mu V^2/(8L^3)$$

where ε represents the dielectric constant of the metal, and μ is the carrier mobility, *V* is the voltage drop across the device and *L* is the thickness of the active layer.

3. Results and discussion

3.1. Synthesis and characterization

The chemical structures and synthetic approaches of polymers PSeBDDIDT and PTzBDDIDT are shown in Scheme 1. Tributyl(selenophen-2-yl)stannane **1** and 2-(tributylstannyl)thiazole **2** were synthesized and used directly without further purification. Monomer **6** and **7** were prepared by Stille coupling of 2BrBDD **3** and **1** or **2** followed by the NBS bromination. Polymers PSeBDDIDT and PTzBDDIDT were obtained by Stille polymerization between monomer **6** or **7** and IDT-Sn, with $Pd(PPh_3)_4$ as the catalyst. The chemical structure of the monomer and the intermediates in the synthesis process were carefully characterized by ^{1}H NMR and ^{13}C NMR spectroscopy. The compound **3** was synthesized according to the previously reported method [37]. The chemical structures of the two polymers were characterized by ^{1}H NMR spectroscopy. Polymers obtained showed good solubility in tetrahydrofuran (THF), chlorobenzene (CB) and o-dichlorobenzene (*o*-DCB) at room temperature. The number average molecular weights (M_n) and polydispersity index (PDI) of PSeBDDIDT and PTzBDDIDT, estimated by gel permeation chromatography (GPC) with tetrahydrofuran as the eluent and polystyrene as the standard, were 25.3 kDa/2.06 and 28.5 kDa/1.98, respectively. As shown in Fig. S1, the thermal properties of two polymers were measured by thermogravimetric analysis (TGA) and the decomposition temperatures (T_d) with 5% weight loss for PSeBDDIDT and PTzBDDIDT are confirmed to be 409 °C and 404 °C, respectively, slightly higher than that of PThBDDIDT (see ref 37).

3.2. Optical and electrochemical properties

The UV–vis absorption spectra of polymers are measured in dilute *o*-DCB solutions and as thin films and the corresponding data are collected in Table 1. As shown in Fig. 1a, three polymers exhibit different absorption feature. It is obvious that the different properties of π-bridges do influence the feature of intermolecular charge transfer (ICT) effect. In contrast of polymer PThBDDIDT, the absorption of polymers PSeBDDIDT and PTzBDDIDT in solutions exhibit red-shifted spectra by about 78 nm and 46 nm respectively. However, different from PThBDDIDT, both polymers PSeBDDIDT and PTzBDDIDT show a strong 0–0 peak (λ_{0-0}) together with a weak 0–1 peak (λ_{0-1}) ICT absorption, implying that there should be strong inter-chain aggregation [38,39]. As shown in Fig. 1b, the temperature-dependent UV–vis absorption spectra of two polymers in dilute solutions were further recorded from 10 to 90 °C to evaluate the aggregation properties. It can be observed that the intensity of 0–0 peak still stronger than that of 0–1 peak even heating at 90 °C, which indicates the aggregation was not broken completely. The above results clearly demonstrate the existence of strong intermolecular stacking even in hot dilute solution for the PSeBDDIDT and PTzBDDIDT polymer and the tuning effect of π-bridges on molecular interactions.

Fig. 1c demonstrates the absorption spectra of three polymers as thin films, accompanied by a red-shift of several nanometers than those in solutions. Also, the absorption of PTzBDDIDT and PThBDDIDT

Table 1
Decomposition temperatures, optical properties and frontier energy levels of polymers.

Polymers	T_d[a]	λ_{max}(nm)		E_g^{opt}[b]	HOMO/LUMO (eV)
	(°C)	solution	film	(eV)	CV[c]
PSeBDDIDT	409	625	632	1.76	−5.40/-3.64
PTzBDDIDT	404	593	597	1.86	−5.67/-3.81

[a] Measured under N_2 atmosphere.
[b] Calculated based on the onset of thin films absorption spectra.
[c] Calculated from cyclic voltammograms curves.

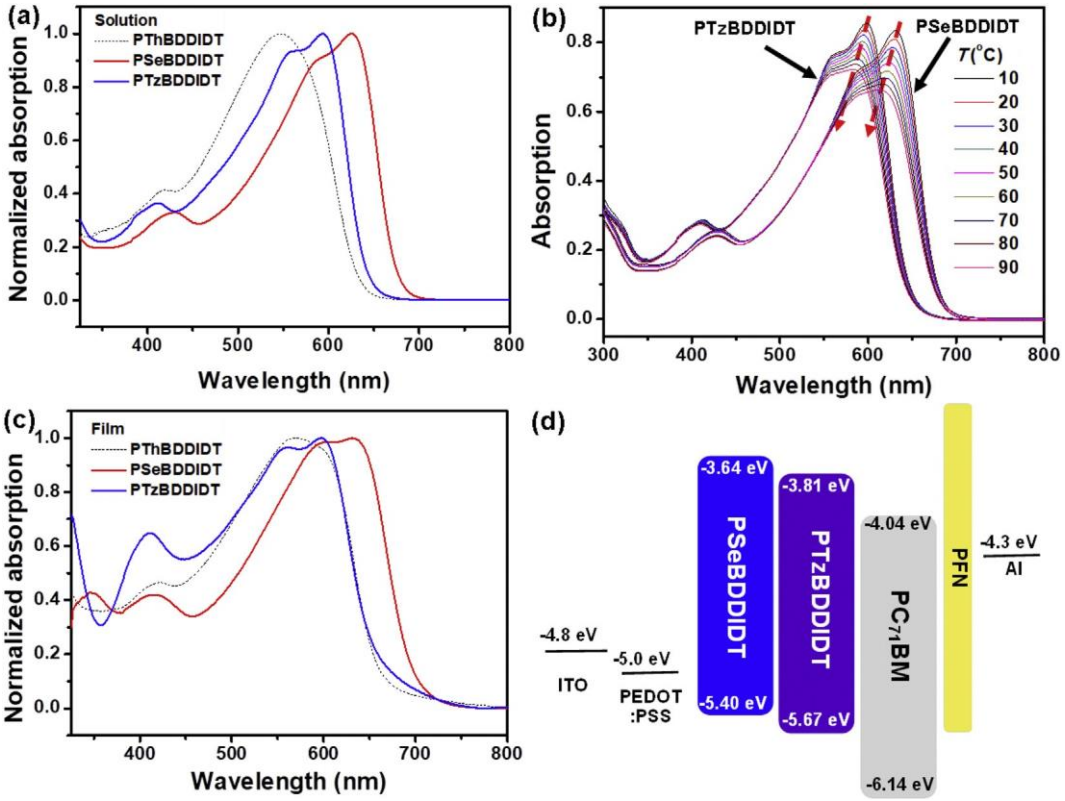

Fig. 1. (a and b) The Uv–vis absorption spectra of polymers in dilute *o*-DCB solutions at room temperature and varying temperatures, respectively; (c) the absorption spectra of polymers as thin films; (d) the energy levels of polymers and the energy level diagrams of materials in polymers solar cells.

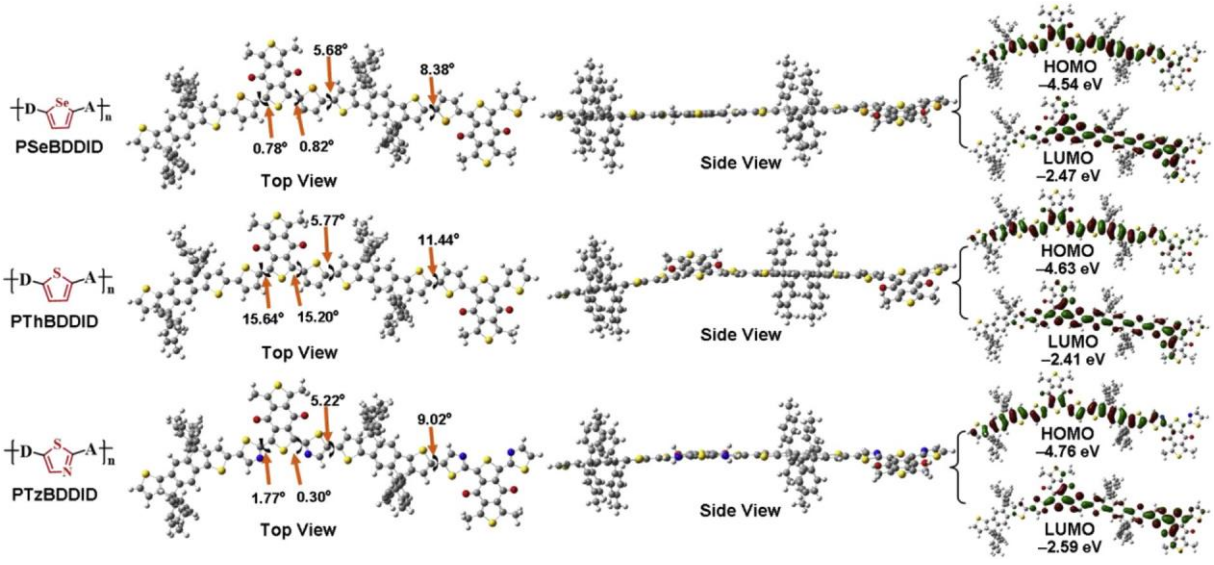

Fig. 2. Theoretically calculated model molecules, corresponding torsion angles, and calculated frontier energy levels of three polymers.

possess the adjacent onset wavelength and identical optical band-gaps (1.86 eV and 1.85 eV, respectively). The greatly red-shifted absorption range of PSeBDDIDT would help harvest more photons and generate high photocurrent. From the onset of thin film absorption spectra, the optical band-gap of polymer PSeBDDIDT was calculated to be 1.76 eV. Electrochemical cyclic voltammetry (CV) measurement was performed to measure the oxidation potentials and further estimate highest occupied molecular orbital (HOMO) energy levels of polymers. The CV curves are displayed in Fig. S2 and the relevant data were collected in Table 1.

From the onset of the oxidation potentials of CV curves, the HOMO energy levels of PSeBDDIDT and PTzBDDIDT were calculated to be −5.40 and −5.76 eV, respectively. Combined with the optical band-gaps, the LUMO energy levels of PSeBDDIDT and PTzBDDIDT were determined to be −3.64 and −3.81 eV, respectively. Compared to polymer PThBDDIDT, PSeBDDIDT reveals upshifted HOMO/LUMO energy levels and PTzBDDIDT reveals downshifted energy levels [37]. This is accessible considering from the electronegativity properties of selenophene and thiazole units. The decreased HOMO level of PTzBDDIDT could promise a high open-circuit voltage in the resulting

PSC. However, it is alarming that the accompanying downshifted LUMO energy level of PTzBDDIDT generated a reduced difference with the acceptor $PC_{71}BM$ (0.23 eV) which could lead to insufficient driving force for exciton separation.

3.3. Theoretical calculations

To provide further insights into the molecular energy levels and molecular conformations of the polymers, theoretical calculations were performed with density functional theory (DFT) at the B3LYP/6-31G level. The long alkyl side chains were replaced with methyl groups to reduce the calculation time. To increase the accuracy of calculation, two repeat unit of every polymer was employed to perform the calculations. As shown in Fig. 2, the dihedral angles between IDT core and neighboring thiophene units are close in three dimers. While great difference of dihedral angles between the BDD unit and neighboring thiophene units was observed. For PSeBDDIDT, the respective dihedral angles were largely suppressed from above 15° to less than 1°, when the π-bridge of D-π-A polymer was transferred from thiophene to selenophene. This manifests a distinct improvement of polymer backbone planarity originating from the relatively larger polarizable radius of selenium atom and stronger $n \rightarrow \sigma^*$ orbital interactions between the oxygen atom on carbonyl group and selenium atom on selenophene bridge [40]. The similar results were found for polymer PTzBDDIDT with the dihedral angles between BDD core and the adjacent thiazole bridges lower than 2° probably induced by the S···N weak interactions between the nitrogen on thiazole and the adjacent sulfur atom on BDD [28]. The side views of three dimers present a more intuitive understanding about the fine-tuning effect of π-bridges on molecular conformations. Generally, the good planarity of polymer backbone would facilitate the better molecular interactions and charge transport in BHJ blends affording for a high photocurrent [41]. Besides, the distributions of HOMO and LUMO energy orbitals of three polymers are also shown in Fig. 2. The electron cloud of HOMO and LUMO frontier orbitals are mainly distributed along the conjugated backbone proportionally, and the calculated energy level values reveal a uniform trend with the results of electrochemical studies.

3.4. Photovoltaic properties and analysis

The single BHJ-polymer solar cells were fabricated with a conventional device structure of ITO/PEDOT:PSS/polymeric donor:$PC_{71}BM$/PFN/Al (see Fig. 3a). The photovoltaic devices were measured under a simulated AM 1.5G illumination of 100 mW cm^{-2}. By varying the polymer/$PC_{71}BM$ weight ratio (w/w) in a broad range, the optimal donor/acceptor weight ratios between PSeBDDIDT or PTzBDDIDT and $PC_{71}BM$ were identified as 1:1. The relevant results at different weight ratios and optimization conditions were collected in Table S1 and Table 2.

The reported device with PThBDDIDT as the polymeric donor revealed a relatively high fill factor (0.68), moderate J_{SC} (11.38 mA cm^{-2}) and generated a best PCE of 7.04% at donor/acceptor w/w = 1:4 [37]. Nevertheless, the optimal w/w was detected to be 1:1 for polymer PSeBDDIDT based devices with greatly improved J_{SC} of 16.04 mA cm^{-2} which should be attributed to the expanded absorption spectra and enhanced intermolecular interactions. As a consequence, the corresponding champion PCE reached 8.65% despite with a decreased FF (0.60) and slightly reduced V_{OC} (0.899 V). To the best of our knowledge, this is the highest efficiency among all the IDT-based polymeric donors reported up to now (see Table S2). However, inferior results were observed from polymer PTzBDDIDT fabricated polymer solar cells. The devices at all measured weight ratios (1:1 to 1:4) exhibited low efficiencies with maximum PCE of 2.75%, which was mainly harmed by the low fill factor as well as photocurrent. In contrast to the counterpart polymer PThBDDIDT, PTzBDDIDT possesses the similar absorption spectra, improved molecular interactions and deeper HOMO energy level. The upshifted V_{OC} of device is consistent with the decreased HOMO energy level of polymer. While the low FF and J_{SC} parameters of PSCs probably be correlated by the narrow LUMO energy difference between the donor and acceptor and the resulting insufficient driving force for exciton separation. To make a clear comparison of the tailor effect of π-bridges on photovoltaic performance, the optimal *J-V* curves of three PSCs are collect in Fig. 3b. The external quantum efficiencies (EQEs) of the polymer solar cells under optimal conditions are shown in Fig. 3c. Moreover, as shown in Table 2, the integrated current densities (J_{SC}^{EQE}) from the EQE spectra are consistent with J_{SC} from the *J-V* measurements, with small deviation of around 5%.

To better evaluate the charge transport behaviors inside PSCs, charge-carrier mobilities were characterized by the space-charge limited current (SCLC) method. Two device structure ITO/PEDOT:PSS/active layer/MoO_3/Al and ITO/ZnO/active layer/PFN/Al were used as electron-only and hole-only devices, respectively. The *J-V* plots from SCLC were displayed in Fig. S3 and the respective hole mobility (μ_h) and electron mobility (μ_e) of every device were collected in Table 2. As shown in Table 2, relatively high and balanced hole and electron mobilties are detected from PThBDDIDT and PSeBDDIDT based devices. While low hole mobility of 0.31×10^{-4} $cm^2 V^{-1}$ s^{-1} exists in PTzBDDIDT based device accompanying with unbalanced electron/hole mobility ratio ($\mu_e/\mu_h = 3.2$). The low and unbalanced charge mobility should be responsible for the low J_{SC}, FF as well as the PCE of the corresponding solar cells. Simultaneously, the series resistance (R_s) and shunt resistance (R_{sh}) are recorded from their respective *J-V* curves under illumination. Generally speaking, a smaller R_s suggests that there is a favorable charge-carrier transport within the PSCs. Meanwhile, a larger R_{sh} suggests that the reverse current densities from the conventional devices are greatly diminished [42]. As shown in Table 2, PSeBDDIDT based device showed low R_s (77 Ω cm^{-2}) and high R_{sh} (5625 Ω cm^{-2}) values, suggesting a good overall diode characteristics. While a high R_s up to 715 cm^{-2} and low R_{sh} of 2114 Ω cm^{-2} were found in PTzBDDIDT based device, indicating inferior charge transport and high reverse current densities in solar cells. This can further proved by the measurement of dark current nature of solar cells. As shown in Fig. 3d, the lowest dark saturation current density J_o of PSeBDDIDT device is 1.05×10^{-9} mA cm^{-2}, while the J_o of PTzBDDIDT device reaches up to 1.85×10^{-8} mA cm^{-2}. This indicates bad diode characteristics occurred in PTzBDDIDT fabricated photovoltaic devices consistent with the low hole and electron charge mobilities as mentioned above.

3.5. BHJ morphology properties

Considering that the photovoltaic performance has a great correlation with the BHJ morphology properties, atomic force microscopy (AFM) and transmission electron microscope (TEM) measurements were applied to study the nature of blends and probe the striking difference of photovoltaic performance of selenophene and thiazole tailored polymers. The AFM and TEM images of PSeBDDIDT/PCBM and PTzBDDIDT/PCBM blend films (1:1, w/w) are shown in Fig. 4. Uniform and smooth blends were detected for PSeBDDIDT/PCBM and PTzBDDIDT/PCBM blend films with small root-mean-square (RMS) roughness of 0.682 nm and 0.833 nm, respectively. Additionally, from the respective TEM images, we can also observe two blends reveal morphology properties with similar polymer aggregations and nanoscale phase separation beneficial for exciton diffusion to the donor/acceptor interface and charge transport. Thus the reasonable BHJ morphologies of two PSC devices probably cannot induce the striking difference of photovoltaic performance especially the rather low fill factor of PTzBDDIDT device.

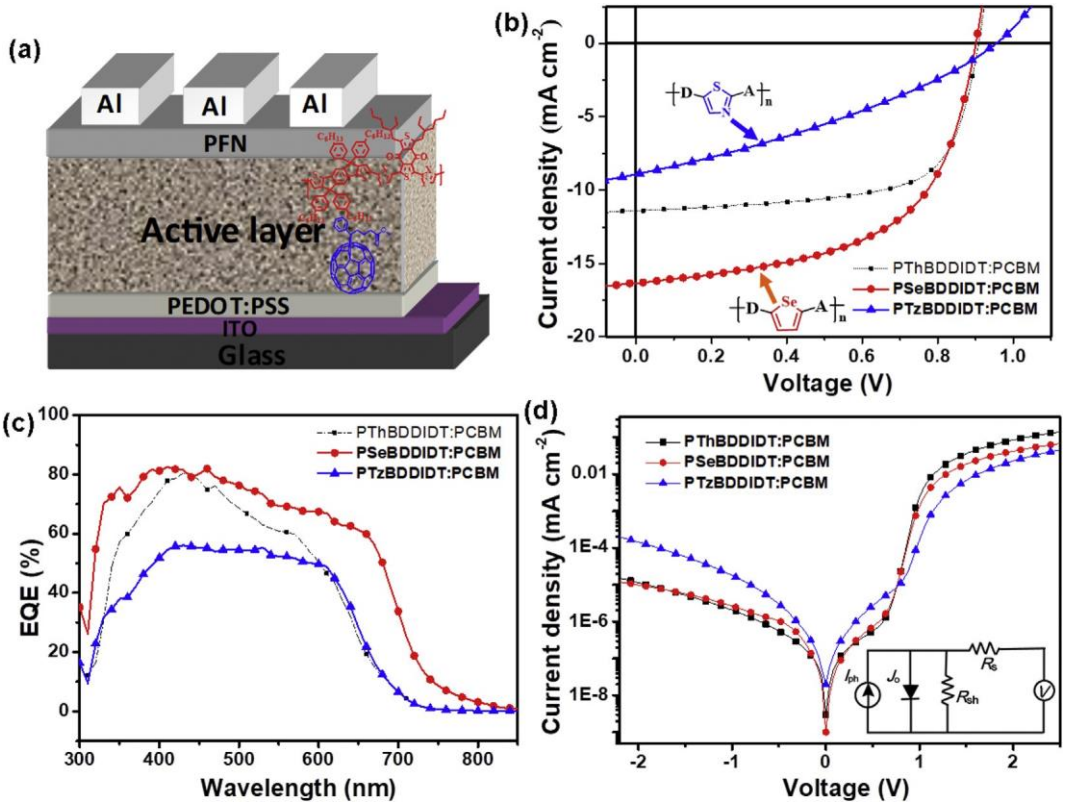

Fig. 3. The devices structure of polymers solar cells (a); the *J-V* (b) curves and EQE curves (c) of the champion devices; (d) dark currents curves of the polymer solar cells, the inset shows the equivalent circuit of the devices.

3.6. Exciton dissociation studies

In order to make a further insight of the working mechanism of PSCs, we investigated the charge separation behaviors of three polymer solar cells. The exciton dissociation probability [$P_{diss}(E,T)$] was measured from the photocurrent density (J_{ph})–effective voltage (V_{eff}) data where J_{ph} is the difference between the light and dark current densities ($J_{ph} = J_L - J_D$) and V_{eff} is the difference between the applied voltage V_a and the voltage V_0 (when J_{ph} is zero) ($V_{eff} = V_0 - V_a$) [43,44]. As shown in Fig. 5a, for PSeBDDIDT/PCBM and PThBDDIDT/PCBM devices, J_{ph} quasi-linearly increased with the voltage at a low value of effective voltage and then saturated at a sufficiently high value of effective voltage. While the J_{ph} of PTzBDDIDT/PCBM device cannot approach the saturation point even applied a high effective voltage up to 5 V, implying low light harvesting in the active layer. Then the exciton dissociation probabilities [$P_{diss}(E,T)$] of three devices, which are related to the electric field (E) and temperature (T) are calculated. In the polymer solar cells, the active layer harvests photons followed by the generation of excitons, while only a portion of the excitons can be dissociated into free carriers. The values of [$P_{diss}(E,T)$] can be calculated from the normalized photocurrent density (J_{ph}/J_{sat}) with respect to V_{eff} [45]. As revealed in Fig. 5b, under the short-circuit conditions ($V_a = 0$ V), efficient exciton dissociation probability of PSeBDDIDT/PCBM and PThBDDIDT/PCBM devices are obtained up to 80% and 89%, respectively. The [$P_{diss}(E,T)$] value of PTzBDDIDT/PCBM device was also rough evaluated considering its uncertain saturated current density even at high effective voltage. Despite this, the PTzBDDIDT/PCBM device exhibited a rather low [$P_{diss}(E,T)$] of 38%, suggesting the great majority of photo-generated excitons failed to be dissociated into free carriers. This is also consistent with the inferior charge transport behaviors in the vertical direction of device, based on SCLC measurement (see Table 2).

4. Conclusions

In summary, two new D-π-A conjugated polymers PSeBDDIDT and PTzBDDIDT based on IDT as the D and BDD as the A unit with different π-bridges selenophene and thiazole, respectively, were prepared and developed for photovoltaic applications. With the previous polymer PThBDDIDT as the counterpart, the tailoring effect of π-bridges on the

Table 2
Device parameters of PSCs under optimal weight ratio and mobility based on SCLC.

Active layer	V_{OC}	J_{SC}	J_{SC}^{EQE}[a]	FF	PCE[b]	R_s[c]	R_{sh}[c]	μ_h[d]	μ_e[d]	
	(V)	(mA cm^{-2})		(%)	(Ω cm^{-2})	(10^{-4} cm^2 V^{-1} s^{-1})				
PThBDDIDT/PC71BM	0.910	11.38	11.04	0.68	7.04 (6.93)	62	8900	4.28	4.25	Ref [37]
PSeBDDIDT/$PC_{71}BM$	0.899	16.04	15.68	0.60	8.65 (8.39)	77	5625	2.43	3.32	This work
PTzBDDIDT/$PC_{71}BM$	0.968	8.12	7.67	0.35	2.75 (2.58)	715	2114	0.31	0.98	This work

[a] Integrated from EQE spectra.
[b] Data were provided in highest (average) format based on more than 10 devices.
[c] Data are obtained from *J-V* curves under illumination.
[d] Based on SCLC measurement.

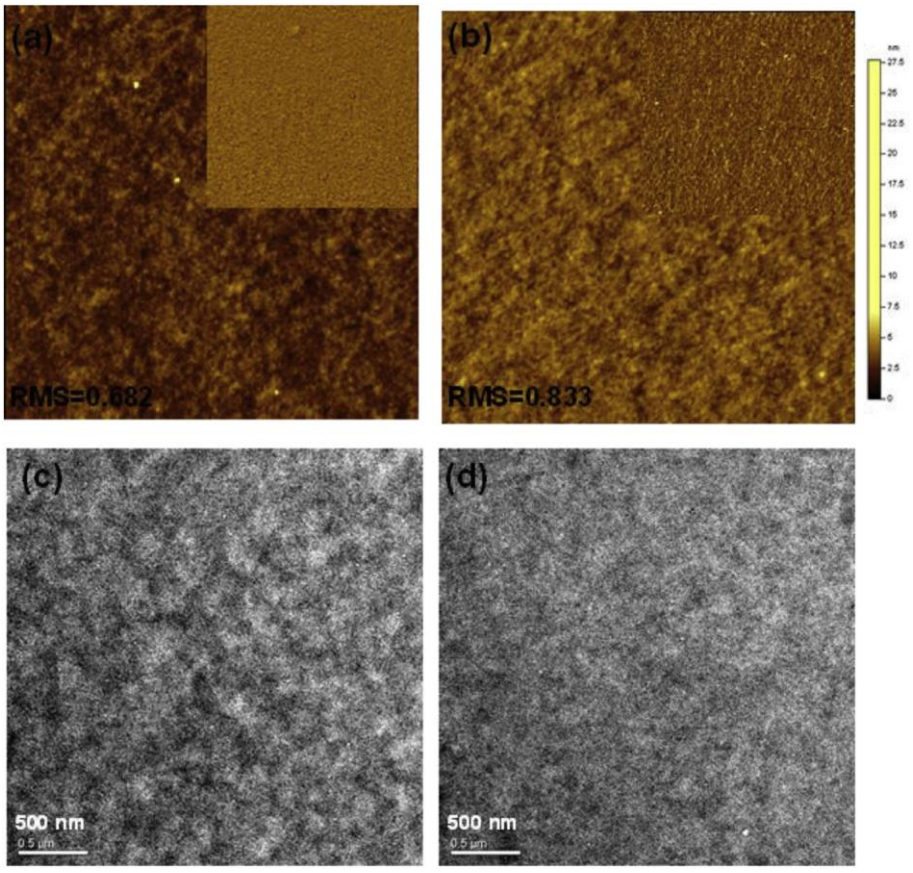

Fig. 4. AFM topography image (5 μm× 5 μm)) of (a) the PSeBDDIDT/PCBM and (b) PTzBDDIDT/PCBM blend films (the unit of RMS is nm), the inner images are the respective phase images. The TEM images of (c) the PSeBDDIDT/PCBM and (d) PTzBDDIDT/PCBM blend films (1:1, w/w). The scale bar of was 500 nm.

basic properties of D-π-A polymers and their photovoltaic properties were detailed and systematically investigated. The theoretical simulations reveal that both polymer PSeBDDIDT and PTzBDDIDT possess a more rigid and planar backbone than PThBDDIDT, originating from the weak interactions between the π-bridge and adjacent BDD unit. The difference of absorption spectra, molecular conformations and frontier energy levels do prove the effective tailoring effect on polymer basic properties. Polymer solar cells were fabricated with polymers as the donor and $PC_{71}BM$ as the acceptor. Devices based on PSeBDDIDT generated the highest efficiency of 8.65% among all the IDT-based polymeric donors, with V_{OC} of 0.899 V, J_{SC} of 16.04 mA cm^{-2} and FF of 0.60. However, poor efficiency was recorded with PTzBDDIDT as the donor materials. The devices exhibit a maximum PCE of 2.75% with V_{OC} of 0.968 V, J_{SC} of 8.12 mA cm^{-2} and FF of 0.35. The results show that the inferior fill factor and efficiency should be attributed to the poor exciton dissociation probability and low charge mobilities which maybe correlated with the insufficient driving force for exciton separation. This work reported a highly efficient IDT-based polymeric donor material and clearly demonstrates the great tailoring effect and rational regulation of π-bridge on the D-π-A polymer properties as well as the efficiency of PSCs.

Conflicts of interest

There are no conflicts to declare.

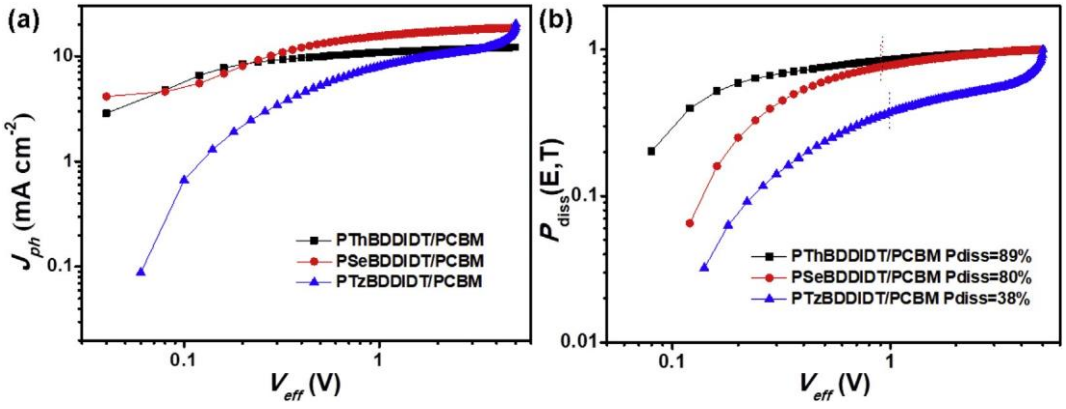

Fig. 5. (a) Photocurrent density (J_{ph}) plotted with respect to effective bias (V_{eff}) for the three photovoltaic devices. (b) Exciton dissociation probability [P_{diss}(E,T)] plotted with respect to effective bias (V_{eff}) for three devices.

Acknowledgement

The authors are deeply grateful to the National Natural Science Foundation of China (21502205, 51573205 and 51773220), Natural Science Foundation of Shandong Province (ZR2018MEM023), Qingdao Source Innovation Plan Applied Basic Research Project (18-2-2-28-jch) and Fundamental Research Funds for the Central Universities (201822002) for the financial support.

Appendix A. Supplementary data

Supplementary data to this article can be found online at https://doi.org/10.1016/j.dyepig.2018.10.008.

References

[1] Ostroverkhova O. Organic optoelectronic materials: mechanisms and applications. Chem Rev 2016;116:13279–412.
[2] Liu Z, Zhang G, Zhang D. Modification of side chains of conjugated molecules and polymers for charge mobility enhancement and sensing functionality. Acc Chem Res 2018;51:1422–32.
[3] Gao Yueyue, Che An, Wang Zhen, Sun Yanming, Wei Zhixiang, Guo Fengyun, Yang Yulin, Zhao Liancheng, Zhang Yong. Efficient post-treatment-free polymer solar cells from indacenodithiophene and fluorinated quinoxaline-based conjugated polymers. Dyes Pigments 2018;154:164–71.
[4] Lin Y, Li Y, Zhan X. Small molecule semiconductors for high-efficiency organic photovoltaics. Chem Soc Rev 2012;41:4245–72.
[5] Yao H, Ye L, Zhang H, Li S, Zhang S, Hou J. Molecular design of benzodithiophene-based organic photovoltaic materials. Chem Rev 2016;116:7397–457.
[6] Mayer A-C, Scully S-R, Hardin B-E, Rowell M-W, McGehee M-D. Semiconductors for organic transistors. Mater Today 2007;10:28–37.
[7] Li S, Ye L, Zhao W, Yan H, Yang B, Liu D, Li W, Ade H, Hou J. A wide band-gap polymer with a deep HOMO level enables 14.2% efficiency in polymer solar cells. J Am Chem Soc 2018;140:7159–67.
[8] Cui C, Wong W-Y, Li Y. Improvement of open-circuit voltage and photovoltaic properties of 2D-conjugated polymers by alkylthio substitution. Energy Environ Sci 2014;7:2276–84.
[9] Kitamura C, Tanaka S, Yamashita Y. Design of narrow-bandgap polymers. syntheses and properties of monomers and polymers containing aromatic-donor and *o*-quinoid-acceptor units. Chem Mater 1996;8:570–8.
[10] Li W, Roelofs W-S, Wienk M-M, Janssen R-A. Enhancing the photocurrent in diketopyrrolopyrrole-based polymer solar cells via energy level control. J Am Chem Soc 2012;134:13787–95.
[11] Qin T, Zajaczkowski W, Pisula W, Baumgarten M, Chen M, Gao M, Wilson G, Easton C-D, Mullen K, Watkins S-E. Tailored donor–acceptor polymers with an A–D1–A–D2 structure: controlling intermolecular interactions to enable enhanced polymer photovoltaic devices. J Am Chem Soc 2014;136:6049–55.
[12] Zhu T, Liu D, Zhang K, Li Y, Liu Z, Gao X, Bao X, Sun M, Yang R. Rational design of asymmetric benzodithiophene based photovoltaic polymers for efficient solar cells. J Mater Chem 2018;6:948–56.
[13] Li W-W, Hendriks K-H, Wienk M-M, Janssen R-A. Diketopyrrolopyrrole polymers for organic solar cells. Acc Chem Res 2016;49:78–85.
[14] Bettencourt-Dias A de, Poloukhtine A. Phenylthiophene—Dipicolinic acid-based emitters with strong solution blue and solid state green emission. J Phys Chem B 2006;110:25638–45.
[15] Zhang Z-G, Wang J. Structures and properties of conjugated Donor–Acceptor copolymers for solar cell applications. J Mater Chem 2012;22:4178–87.
[16] Chen S, Yao H, Li Z, Awartani O-M, Liu Y, Wang Z, Yang G, Zhang J, Ade H, Yan H. Surprising effects upon inserting benzene units into a quaterthiophene-based D-A polymer–improving non-fullerene organic solar cells via donor polymer design. Adv Energy Mater 2017;7:1602304.
[17] Kim J-H, Park J-B, Shin S-A, Hyun M-H, Hwang D-H. Low-bandgap copolymers consisting of 2,1,3-benzoselenadiazole and carbazole derivatives with thiophene or selenophene π-bridges. Polymer 2014;55:3605–13.
[18] Uy R-L, Yan L, Li W, You W. Tuning fluorinated benzotriazole polymers through alkylthio substitution and selenophene incorporation for bulk heterojunction solar cells. Macromolecules 2014;47:2289–95.
[19] Chen H-Y, Yeh S-C, Chen C-T, Chen C-T. Comparison of thiophene- and selenophene-bridged donor–acceptor low band-gap copolymers used in bulk-heterojunction organic photovoltaics. J Mater Chem 2012;22:21549–59.
[20] Lee K-C, Park W-T, Noh Y-Y, Yang C. Benzodipyrrolidone (BDP)-Based polymer semiconductors containing a series of chalcogen atoms: comprehensive investigation of the effect of heteroaromatic blocks on intrinsic semiconducting properties. ACS Appl Mater Interfaces 2014;6:4872–82.
[21] Patra A, Bendikov MJ. J Mater Chem 2010;20:422–33.
[22] Xu Z, Fan Q-P, Meng X-Y, Guo X, Su W-Y, Ma W, Zhang M-J, Li Y-F. Selenium-containing medium bandgap copolymer for bulk heterojunction polymer solar cells with high efficiency of 9.8%. Chem Mater 2017;29:4811–8.
[23] Bronstein H, Collado-Fregoso E, Hadipour A, Soon Y-W, Huang Z, Dimitrov S-D, Ashraf R-S, Rand B-P, Watkins S-E, Tuladhar P-S, Meager I, Durrant J-R, McCulloch I. Thieno[3,2-*b*]thiophene-diketopyrrolopyrrole containing polymers for inverted solar cells devices with high short circuit currents. Adv Funct Mater 2013;23:5647–54.
[24] Duan C, Franeker J, Wienk M-M, Janssen R. High open circuit voltage polymer solar cells enabled by employing thiazoles in semiconducting polymers. Polym Chem 2016;7:5730–8.
[25] Lee J-Y, Song K-W, Song H-J, Moon D-K. Synthesis and photovoltaic property of donor–acceptor type conjugated polymer containing carbazole and 4,7-dithiazolylbenzothiadiazole moiety utilized as a promising electron withdrawing unit. Synthetic Met 2011;161:2434–40.
[26] Zaborova E, Chavez P, Bechara R, Leveque P, Heiser T, Mery S, Leclerc N. Thiazole as a weak electron-donor unit to lower the frontier orbital energy levels of donor–acceptor alternating conjugated materials. Chem Commun (J Chem Soc Sect D) 2013;49:9938–40.
[27] Zhu D, Bao X, Zhu Q, Gu C, Qiu M, Wen S, Wang J, Shahid B, Yang R. Thienothiophene-based copolymers for high-performance solar cells, employing different orientations of the thiazole group as a π bridge. Energy Environ Sci 2017;10:614–20.
[28] Yu S, Chen Y, Yang L, Ye P, Wu J, Yu J, Zhang S, Gao Y, Huang H. Significant enhancement of photovoltaic performance through introducing S···N conformational locks. J Mater Chem 2017;5:21674–8.
[29] Dang D, Chen W, Himmelberger S, Tao Q, Lundin A, Yang R, Zhu W, Salleo A, Müller C, Wang E. Enhanced photovoltaic performance of indacenodithiophene-quinoxaline copolymers by side-chain modulation. Adv Energy Mater 2014;4:1400680.
[30] Gao W, Liu T, Hao M, Wu K, Zhang C, Sun Y, Yang C. Dithieno[3,2-*b*:2′,3′-*d*]pyridin-5(4*H*)-one based D–A type copolymers with wide bandgaps of up to 2.05 eV to achieve solar cell efficiencies of up to 7.33%. Chem Sci 2016;7:6167–75.
[31] Guo X, Zhang M, Tan J, Zhang S, Huo L, Hu W, Li Y, Hou J. Influence of D/A ratio on photovoltaic performance of a highly efficient polymer solar cell system. Adv Mater (Weinheim, Ger) 2012;24:6536–41.
[32] Ma Y, Chen S-C, Wang Z, Ma W, Wang J, Yin Z, Tang C, Cai D, Zheng Q. Indacenodithiophene-based wide bandgap copolymers for high performance single-junction and tandem polymer solar cells. Nanomater Energy 2017;33:313–24.
[33] Wang C, Xu X, Zhang W, Bergqvist J, Xia Y, Meng X, Bini K, Ma W, Yartsev A, Vandewal K, Andersson M-R, Inganäs O, Fahlman M, Wang E. Low band gap polymer solar cells with minimal voltage losses. Adv Energy Mater 2016;6:1600148.
[34] Yu Junting, Cao Jiamin, Tan Hua, Peng Wenhong, Wang Yafei, Zhu Weiguo. Structure-performance correlation of indacenodithiophene-based narrow band-gap polymers with pendant diketopyrrolopyrrole units. Dyes Pigments 2017;141:21–8.
[35] Zhang M, Guo X, Wang X, Wang H, Li Y. Synthesis and photovoltaic properties of D–A copolymers based on alkyl-Substituted indacenodithiophene donor unit. Chem Mater 2011;23:4264–70.
[36] Wang Ting, Chen Yanhua, Bao Xichang, Du Zhengkun, Guo Jing, Wang Ning, Sun Mingliang, Yang Renqiang. A new isoindigo-based molecule with ideal energy levels for solution-processable organic solar cells. Dyes Pigments 2013;98:11–6.
[37] Zhu T, Zhang Y, Li Y, Song X, Liu Z, Wen S, Bao X, Sun M, Yang R. Acceptor-rich bulk heterojunction polymer solar cells with balanced charge mobilities. Org Electron 2017;51:16–24.
[38] Li Y, Duan L, Liu D, Chen W, Bao X, Zhen H, Liu H, Yang R. Design of asymmetric benzodithiophene based wide band-gap conjugated polymers toward efficient polymer solar cells promoted by a low boiling point additive. J Mater Chem C 2018;6:2806–13.
[39] Li Y, Wang J, Liu Y, Qiu M, Wen S, Bao X, Wang N, Sun M, Yang R. Investigation of fluorination on donor moiety of Donor–Acceptor 4,7-dithienylbenzothiadiazole-based conjugated polymers toward enhanced photovoltaic efficiency. ACS Appl Mater Interfaces 2016;8:26152–61.
[40] Pascoe D-J, Ling K-B, Cockroft S-L. The Origin of chalcogen-bonding interactions. J Am Chem Soc 2017;139:15160–7.
[41] Kang S-H, Lee H-R, Dutta G-K, Lee J, Oh J-H, Yang C. A role of side-chain regiochemistry of thienylene–vinylene–thienylene (TVT) in the transistor performance of isomeric polymers. Macromolecules 2017;50:884–90.
[42] Li Z, Wang X, Ren J, Gan G, Liu C, Sun Q, Wang H, Hao Y. Fabrication of benzothiadiazole–benzodithiophene-based random copolymers for efficient thick-film polymer solar cells via a solvent vapor annealing approach. J Mater Chem C 2018;6:4555–64.
[43] Wu J-L, Chen F-C, Hsiao Y-S, Huang M-H, Hsu C-S. Surface plasmonic effects of metallic nanoparticles on the performance of polymer bulk heterojunction solar cells. ACS Nano 2011;5:959–67.
[44] Shrotriya V, Yao Y, Li G, Yang Y. Effect of self-organization in polymer/fullerene bulk heterojunctions on solar cell performance. Appl Phys Lett 2006;89:063505.
[45] Yang B, Zhang S, Chen Y, Cui Y, Liu D, Yao H, Zhang J, Wei Z, Hou J. Investigation of conjugated polymers based on naphtho[2,3-*c*]thiophene-4,9-dione in fullerene-based and fullerene-free polymer solar cells. Macromolecules 2017;50:1453–62.